23rd International Conference on Renewable Energies and Power Quality (ICREPQ'25)
Tenerife (Spain), 25th to 27th June 2025
Renewable Energy and Power Quality Journal (RE&PQJ)
ISSN 2172-038 X, Volume No.23, September 2025

Performance Improvement Of Sliding Mode Control In Wind Turbine Application

A. Redouane[1], R. Saou[1] and A. Oukaour[2]

[1] Université de Bejaia, Faculté de Technologie, Laboratoire de Génie Électrique, 06000 Bejaia, Algeria

[2] Laboratoire de Recherche en Sciences du Numérique GREYC, Université de Caen Normandie, 6 Boulevard du Maréchal Juin, 14032 Caen, France

Abstract. This paper introduces a new reaching law for sliding mode control to regulate the current loop of a DC-DC boost converter in a small-scale standalone wind turbine system equipped with battery storage. The wind turbine employs a direct-driven generator known as the Vernier Doubly Salient Permanent Magnet (DSPM) generator. The proposed control aims to minimize the inductor current ripple in the DC-DC boost converter and enhance the overall performance of the wind turbine system. The system's behavior is analyzed through simulations conducted in MATLAB/Simulink. The results indicate that the proposed method achieves reduced current ripple and superior performance compared to the Gao's second law sliding mode control (SMC) approach.

Key words. Renewable energy system, Sliding mode control, Direct driven generator, Wind energy system.

1. Introduction

The integration of renewable energy sources in power systems has received a lot of attention in the last few years, especially wind and solar sources. Due to their high efficiency and relatively low cost of production, wind energy is one of the most significant renewable sources and the fastest growing renewable energy technologies [1]. According to the Energy Institute data on the world energy market, global wind turbine installed capacity has surged from around 300 GW in 2013 to over 1,000 GW by 2023 as illustrated in Fig.1. This remarkable growth highlights not only the rapid expansion of wind energy, but also its crucial role as one of the most promising renewable energy sources in the global energy transition [2].

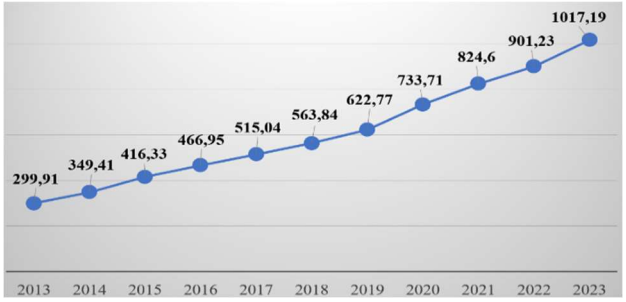

Fig. 1. Global wind turbine installed capacity.[2]

In a conventional wind turbine system configuration as shown in Fig 2, a gearbox is employed to couple the turbine shaft with the generator rotor, such as an induction generator or a synchronous generator [3]. The main function of the gearbox is to increase the rotational speed of the turbine shaft to match the operational requirements of the generator. However, this mechanical component presents several disadvantages, including energy losses, noise, volume, mechanical complexity, maintenance requirements, and expensive installation costs.

Conventional generators, widely used in wind turbine systems, include squirrel-cage induction generators (SCIGs), doubly-fed induction generators (DFIGs), and permanent magnet synchronous generators (PMSGs) [4]. Although each type offers specific advantages, they all share a common drawback related to the limitation imposed by the gearboxes.

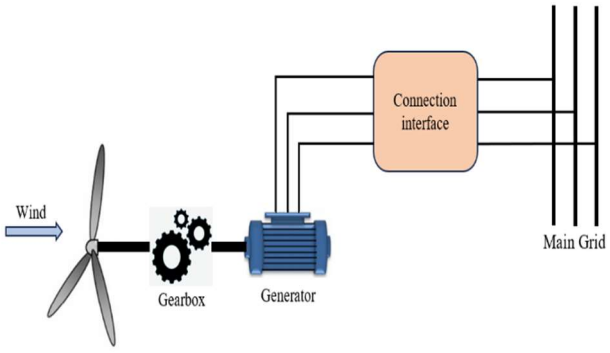

Fig. 2. Conventional wind turbine system.

To overcome this limitation, direct-drive wind turbine systems have been developed, where the turbine shaft is directly coupled to a low-speed generator, eliminating the need for a gearbox as shown in Fig. 3. These systems offer several advantages, including higher overall efficiency, enhanced system reliability, and the elimination of maintenance, energy losses, and noise [5]. However, they typically require a generator with high

pole numbers to achieve the low rotational speeds, and pose specific challenges in terms of generator design.

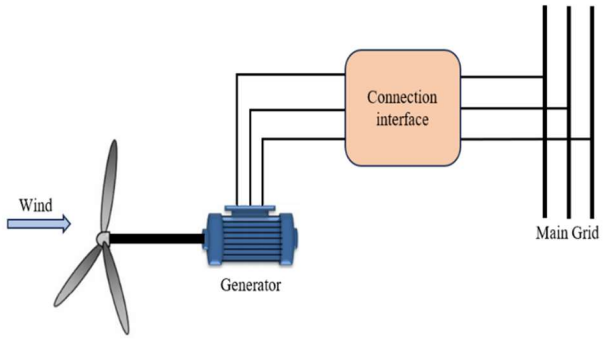

Fig. 3. Direct-drive wind turbine system.

Among the various direct-drive generator technologies, the Vernier Doubly Salient Permanent Magnet (VDSPM) generator stands out as particularly well-suited for low-speed applications. This generator is characterized by a toothed stator and rotor, enabling the generation of a sinusoidal electromotive force and high mechanical torque. As a result, VDSPM generators are highly compatible with direct-drive wind turbines, especially where compactness, robustness, and high torque density are required [6].

While the mechanical design improves system reliability, the control of the energy conversion interface plays a key role in maintaining system stability under varying wind profiles and load conditions. Small-scale wind turbine systems that employ permanent magnet synchronous generators (PMSGs) often utilize a two-stage power conversion configuration, consisting of a three-phase diode bridge rectifier and a DC-DC converter, to ensure efficient energy transfer and voltage regulation in the case of DC electric power distribution systems. The control of the DC-DC converters poses a considerable challenge owing to their inherent nonlinear characteristics. Numerous studies in the literature have addressed various control strategies to manage these complexities. Reference [7] investigates the application of fuzzy logic control for DC-DC converters, addressing computational challenges and proposing a look-up table controller to simplify the control process. Reference [8] details the design of a cascade control system for a DC-DC converter, incorporating a fractional-order PID controller in the outer loop and a self-tuning adaptive controller in the inner loop. Reference [9] introduces a novel backstepping control strategy for a DC-DC boost converter, capable of managing significant load variations and voltage reference changes, and employing disturbance observers to enhance performance. Reference [10] proposes a nonlinear backstepping control approach with integral action for a DC-DC converter, optimized using genetic algorithms. Reference [11] outlines a sliding mode control (SMC) design procedure for DC-DC converters, introducing a chattering reduction approach. Reference [12] presents an integral sliding mode control (ISMC) algorithm designed to mitigate the variable switching frequency problem typically encountered during load and supply variations in DC-DC converters. Reference [5] describes a sliding mode control (SMC) strategy based on Maximum Power Point Tracking (MPPT) and Gao's reaching law to regulate the DC-DC converter current.

This paper investigates a small-scale standalone wind energy system with battery storage, employing a non-conventional direct-drive generator, which represents the first originality of this research work. To maximize power extraction from the wind turbine, a tip speed ratio-based SMC method is utilized. For the DC-DC boost converter, a novel reaching law is proposed to regulate the inner loop. This law aims to reduce the inductor current ripple in the DC-DC boost converter. This represents the second originality of this work. The effectiveness of the proposed control strategy is evaluated through two tests: the first under varying load and wind speed conditions, and the second with changes in converter parameters. Additionally, a comparative analysis is conducted between the proposed technique and Gao's second law sliding mode control (SMC) approach.

2. System Description

The system consists of a direct-driven wind turbine coupled to a three-phase Vernier Doubly Salient Permanent Magnet (V-DSPM) generator. The generator's stator is connected to a three-phase uncontrolled rectifier, with the rectifier's DC bus linked to a DC-DC boost converter. A battery integrated with a bidirectional DC-DC converter is utilized to manage power flow and regulate the DC bus voltage. Finally, the system includes a variable DC load. The overall configuration is depicted in Fig. 4.

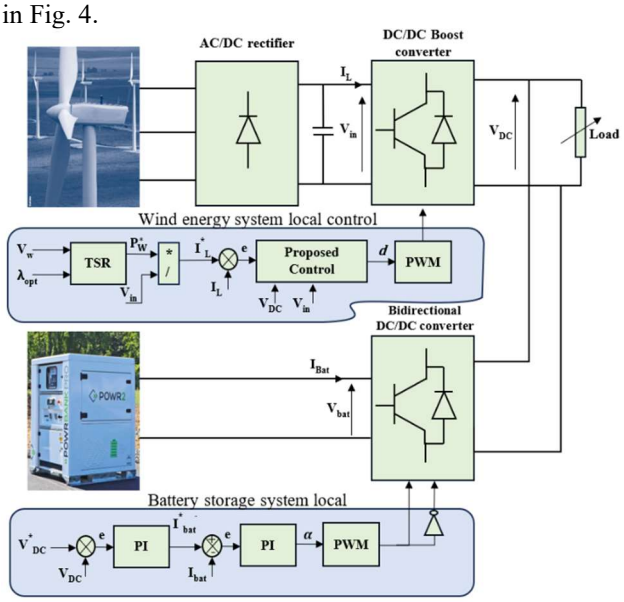

Fig. 4. Standalone wind energy conversion system.

A. Wind turbine modelling

The power captured by the wind turbine can be expressed by the following formula [5]:

$$P_t = \frac{1}{2}\rho\,\pi\,R^2\,C_p(\lambda)\,V_w^3 \qquad (1)$$

The power coefficient (C_p) is a function of the tip speed ratio (λ), which is expressed as:

$$\lambda = \frac{\Omega_t R}{V_w} \quad (2)$$

Where: ρ represents the air density, R the turbine radius, C_p the power coefficient, V_w the wind speed, and Ω_t the mechanical shaft speed of the turbine.

The power coefficient curve $C_p(\lambda)$ is shown in Fig.5, and is expressed, as follows [6]:

$$C_p(\lambda) = 0.03948\lambda^5 - 0.3248\lambda^4 + 0.82919\lambda^3 - 0.70335\lambda^2 + 0.25754\lambda - 0.013889 \quad (3)$$

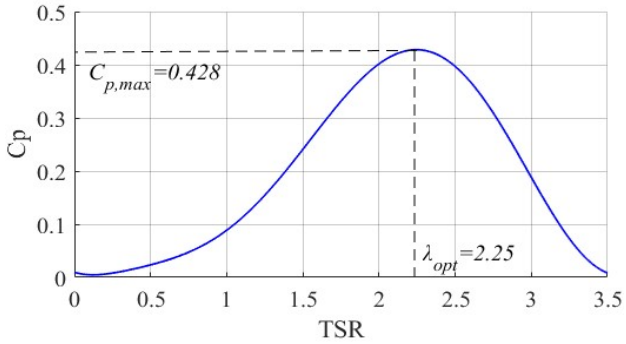

Fig. 5. Power coefficient curve C_p.

B. Vernier DSPM generator modelling

In conventional permanent magnet generators, achieving a high number of poles is challenging due to the rotor topology and the complexity of embedding permanent magnets within the rotor yoke. This drawback limits the ability to operate at very low rotational speeds, as the rotational speed is inversely proportional to the number of poles.

$$\Omega_g = \frac{60\,f}{P} \quad (4)$$

To address this design limitation, the authors of [13] have proposed a direct-drive low-speed Doubly Salient Permanent Magnet (DSPM) generator for wind turbine applications, illustrated in Fig.6. This generator is a three-phase, 10 kW machine characterized by a toothed stator and rotor configuration. The stator comprises N_s= 48 teeth distributed across 12 slots, corresponding to 4 slots per phase. The winding of each phase consists of four concentric coils [4]. The rotor, which is passive, includes N_r= 64 teeth. The excitation is provided by four NdFeB magnets embedded in the stator yoke.

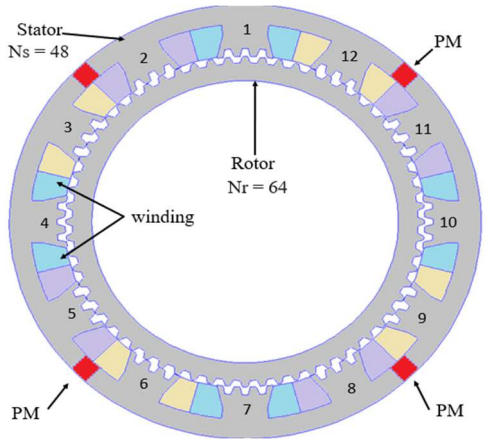

Fig. 6. Axial cross-section of Doubly Salient Permanent Magnet (DSPM) generator.

In this structure, the generator's rotational speed is inversely proportional to the number of rotor teeth N_r, enabling operation at industrial frequency under low-speed conditions. Specifically, for a target frequency of 50 Hz, the generator can operate at a rotational speed of 50 rpm.

$$\Omega_g = \frac{60\,f}{N_r} \quad (5)$$

The main drawback of the DSPM generator is its non-sinusoidal electromotive force waveform, as shown in the Fig. 7 below.

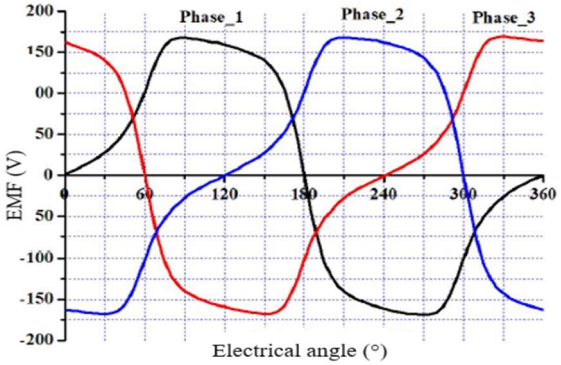

Fig. 7. DSPM electromotive force.

To overcome this limitation, the authors of paper [14] exploited the Vernier effect, which is achieved by designing the rotor tooth pitch τ_r different from the stator tooth pitch τ_s (see Fig.8).

$$\tau_s = \frac{2\pi}{N_{seq}}, \tau_r = \frac{2\pi}{N_r} \quad (6)$$

Where: N_{seq} (different from N_s) represents the number of stator teeth the generator would have if the stator armature were distributed-toothed and not slotted.

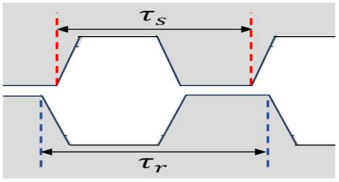

Fig. 8. Rotor and stator teeth.

For effective energy conversion and torque generation, the Vernier DSPM generator must meet the following conditions [6]:

$$\begin{cases} \pm N_{seq} \mp N_r = \pm P \pm P_e \\ \pm N_{seq} \neq 2P \pm 2P_e \\ \pm N_r \neq \pm 2P \pm 2P_e \end{cases} \quad (7)$$

P_e and P represent the number of magnet pairs and slot pairs per phase, respectively. These conditions are satisfied when N_{seq} = 68 and N_{seq} = 60. The generator with N_{seq} = 68 exhibits superior performance, which is why it was selected (see Fig.9).

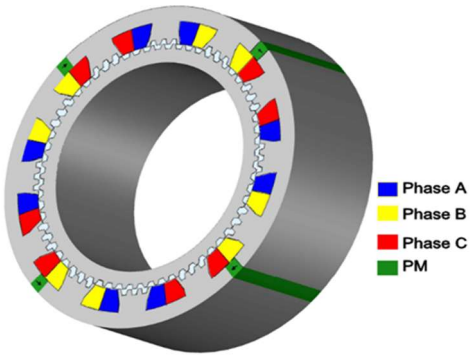

Fig. 9. Cross section of the Vernier DSPMG.

The Vernier DSPM generator with N_{seq}= 68 equivalent stator teeth improves the electromagnetic performance, particularly the electromotive force waveform. As shown in the following Fig.10 below.

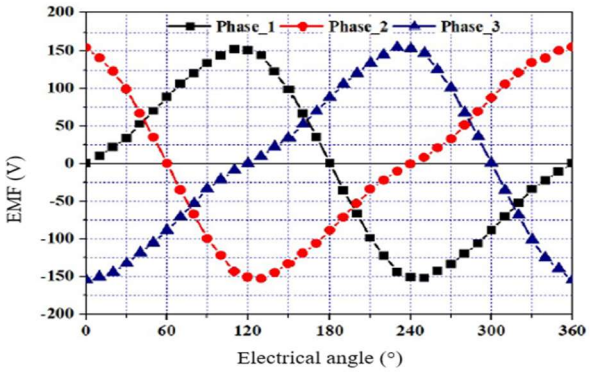

Fig. 10. Vernier DSPM electromotive force.

The mathematical model of the VDSPM generator is simplified through the Fourier transform, where the harmonic order terms greater than 1 are neglected.

Thus, the expressions of the VDSPM generator voltages in the *dq* reference frame are given by [5]:

$$\begin{cases} V_d = -\left(R_s + 2w_e M_{dq}\right) i_d + \frac{w_e}{2}\left(3L_d - L_q\right) i_q - L_d \frac{di_d}{dt} - M_{dq} \frac{di_q}{dt} \\ V_q = -\left(R_s - 2w_e M_{dq}\right) i_q - \frac{w_e}{2}\left(3L_q - L_d\right) i_d - L_q \frac{di_q}{dt} - M_{dq} \frac{di_d}{dt} - \sqrt{\frac{3}{2}} \varphi_1 w_e \end{cases} \quad (8)$$

Where: R_s denotes the stator resistance, while i_d and i_q refer to the direct and quadrature currents. L_d and L_q represent the direct and quadrature inductances, respectively, and M_{dq} denotes the mutual inductance, and φ_1 represents the permanent magnet flux first harmonic, and w_e is the electrical velocity.

With [5]:

$$\begin{cases} L_{dq} = L_0 - M_0 \pm \frac{1}{2}(L_1 + 2M_1) \cos 3\theta_e \\ M_{dq} = -\frac{1}{2}(L_1 + 2M_1) \sin 3\theta_e \\ \theta_e = \int w_e \, dt \end{cases} \quad (9)$$

Where: L_0 and M_0 are the self-inductance and mutual continuous part, L_1 and M_1 are the self-inductance and mutual first harmonic, and θ_e represents the electrical position.

The direct and quadratic magnetic flux are expressed by [5]:

$$\begin{cases} \varphi_d = L_d i_d + M_{dq} i_q + \sqrt{\frac{3}{2}} \varphi_1 \\ \varphi_q = L_q i_q + M_{dq} i_d \end{cases} \quad (10)$$

The electromagnetic torque T_{em} is given by [3]:

$$T_{em} = -\sqrt{\frac{3}{2}} N_r \varphi_1 i_q + \frac{1}{2} N_r \left(L_d - L_q\right) i_d i_q - \frac{1}{2} N_r M_{dq} \left(i_d^2 - i_q^2\right) \quad (11)$$

The active and reactive power are expressed as follow [3]:

$$\begin{cases} P = v_d i_d + v_q i_q \\ Q = v_d i_q - v_q i_d \end{cases} \quad (12)$$

C. *Battery storage modelling*

The R_{int} model is used to represent the lithium-ion battery, as illustrated in Fig. 11. This model characterizes the dynamic behavior of the lithium-ion battery using an ideal voltage source E_{bat} and an internal resistance R_{int} in series.

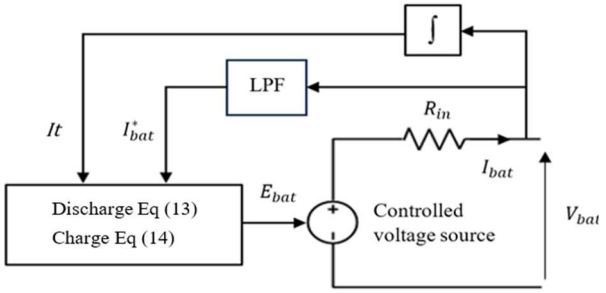

Fig. 11. Equivalent circuit of the lithium-ion battery model.

The battery voltage can be given as follows [6]:

$$V_{bat} = E_{bat} \pm R_{int} I_{bat} \quad (13)$$

Where: V_{bat} and I_{bat} are the battery voltage and current, respectively.

The state of charge SOC can be expressed as follows [15]:

$$SOC\ (t) = SOC_{init} - \frac{1}{Q_{max}} \int_0^t I_{bat}\ dt \quad (14)$$

Where: SOC_{init} denotes the battery initial state of charge, and Q_{max} is the battery maximum capacity.

The discharge and charge equations of the battery can be given as follows [16]:

$$E_{bat,disch} = E_{\text{bat}} - K_{\text{b}}\left(\frac{Q_{max}}{Q_{max}-It}\right) I^*_{bat} - K_{\text{b}}\left(\frac{Q_{max}}{Q_{max}-It}\right) It + A_b\ e^{(-B\cdot It)} \quad (15)$$

$$E_{bat,ch} = E_{\text{bat}} - K_{\text{b}}\left(\frac{Q_{max}}{It+0.1\cdot Q_{max}}\right) I^*_{bat} - K_{\text{b}}\left(\frac{Q_{max}}{Q_{max}-It}\right) It + A_b\ e^{(-B\cdot It)} \quad (16)$$

Where: K_{b} represents the resistance polarization coefficient (Ω), I^*_{bat} denotes the current low-frequency (A), $It = \int I_{bat}\ dt$ represents the extracted capacity (Ah), A_b is the exponential voltage (V) and B is the exponential capacity (Ah^{-1}).

3. Global system control

A. Wind turbine control

To extract the optimal power from wind turbines, the Maximum Power Point Tracking (MPPT) techniques are employed. According to the literature, numerous strategies have been proposed and implemented. The most employed methods include Tip Speed Ratio (TSR) control, Optimal Torque (OT) control, Power Signal Feedback (PSF) control, Perturbation and Observation (P&O) control.
In this study, TSR strategy is selected for its numerous benefits, including its simplicity of implementation, rapid convergence, and high efficiency under fluctuating wind speeds. Fig.12 presents the TSR control scheme.

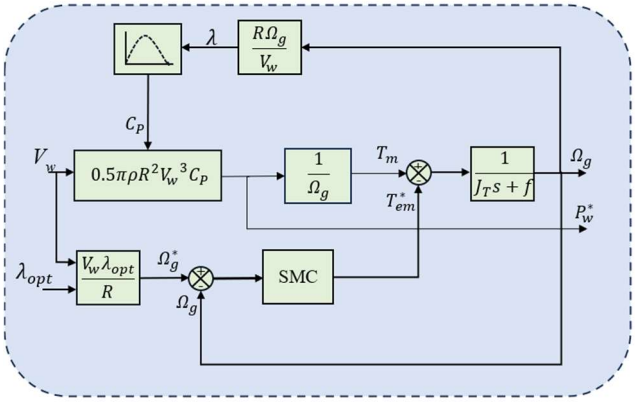

Fig. 12. TSR control scheme.

B. DC-DC boost converter control

Among the control methods used in the literature, the sliding mode control law passes other techniques in terms of tracking accuracy, robustness and against disturbances [17].
To reduce the chattering and improves the performances of the second Goa's law [18], this paper proposes new reaching law (see Fig. 13). The new reaching law is given by:

$$\dot{s} = -k|s|^{0.5}(sign(s) + s) \quad (17)$$

Where: k is sliding mode gain.

Analyzing the new reaching law in Eq (17):

- When $|s|$is is far from the sliding surface, the dynamics of $\dot{s}$ behave similarly to classical sliding mode control, exhibiting a strong control action. This enables the system a fast approach to the sliding surface.

- As $|s|$ approaches to zero, the term $|s|^{0.5}$ becomes smaller and makes the control less sensitive to small changes in $|s|$ as it approaches zero, which helps to reduce the chattering. The system becomes smoother and more stable without rapid, repetitive ocillations around the sliding surface.

In order to analyze the stability of the proposed method. Examine the derivative of the following Lyapunov function $V = 0.5\ s^2$:

$$\dot{V} = s\dot{s} \le 0$$
$$\dot{V} = -s\ k|s|^{0.5}(sign(s)+s) \le 0 \quad (18)$$

If sign(s) = ±1 and k > 0, it can be seen that $\dot{V} \le 0$. Therefore, according to the Lyapunov stability condition, the system is stable.

The inductor current equation of the DC-DC boost converter is given as follow:

$$\frac{dI_L}{dt} = \frac{V_{in}}{L} - (1-d)\frac{V_{DC}}{L} \quad (19)$$

The sliding surface and its derivative are defined as follows:

$$s = I^*_L - I_L$$
$$\dot{s} = \dot{I}^*_L - \dot{I}_L \quad (20)$$

The sliding mode control signal is given as the sum of the equivalent and discontinuous control signals :

$$u = u_{eq} + u_{dis} \quad (21)$$

The proposed discontinous control part is given as follow:

$$\dot{s} = -k|s|^{0.5}(sign(s) + s) \quad (22)$$

By substituting Eq (19) into Eq (20):

$$\dot{s} = -\left[\frac{V_{in}}{L} - (1-d)\frac{V_{DC}}{L}\right] \quad (23)$$

By substituting Eq (23) into Eq (22), the proposed reaching law control signal:

$$d = \frac{V_{DC}-V_{in}}{V_{DC}} + \frac{L.k.|s|^{0.5}(sign(s)+s)}{V_{DC}} \quad (24)$$

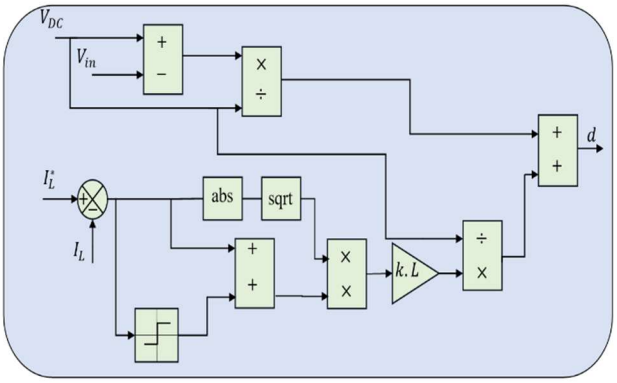

Fig. 13. The proposed control method scheme.

C. Battery stroage system control

A dual control loop is employed to regulate the battery storage system. The DC-Bus reference voltage V_{DC}^* is compared with the measured one V_{DC}, and the resulting error signal is fed into a PI controller. The output of this controller generates the reference battery current I_{bat}^*. Subsequently, a second comparison is made between the actual battery current I_{bat} and the reference battery current I_{bat}^*, with the resulting error signal processed by a second PI controller. The duty cycle of the converter is adjusted according to the output of the second PI controller.

4 . Results and discussion

The standalone wind energy conversion system was simulated within a MATLAB/Simulink environment. The system utilizes a direct-driven generator, specifically the Vernier Doubly Salient Permanent Magnet Generator (V-DSPMG). Additionally, a new reaching law was implemented to regulate the inductor current of the DC-DC boost converter. To evaluate the robustness of the proposed control strategy, two tests were performed.

The first test evaluated the system's performance under varying wind speeds and load conditions, while the second test investigated the effects of parameter variations in the DC-DC boost converter.

Fig. 14. illustrates the VDSPMG speed, showing that the generator speed aligns with its speed reference. Fig. 15. displays the generator direct and the quadratic current.

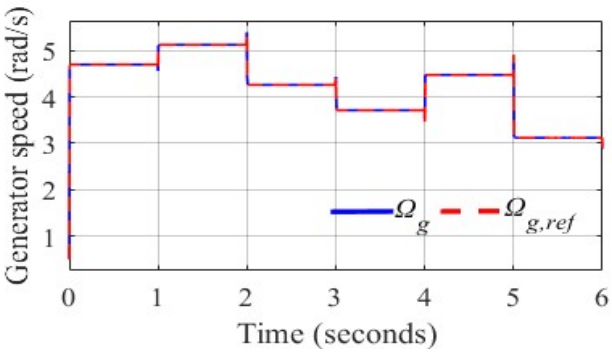

Fig. 14. Generator speed Ω_g.

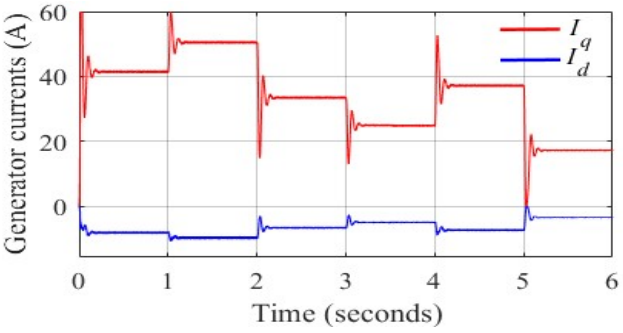

Fig. 15. Generator current.

Fig. 16. presents the simulation results of the DC/DC boost inductor current under two different test scenarios, utilizing the proposed reaching law. The results clearly demonstrate that the proposed control strategy significantly reduces the chattering phenomenon, in contrast to Gao's second reaching law, which exhibits higher oscillations. This improvement highlights the effectiveness of the proposed control in reducing ripple, and ensuring smoother operation.

Additionally, the proposed method shows superior efficiency in the variations of the DC/DC converter parameters. Specifically, from t = 3.5 s, a +50% increase is applied to both the inductor L value and the DC-bus capacitor C_{DC} value.

Despite variations in these parameters, the proposed control effectively adapts and maintains optimal performance.

This performace is achieved while keeping the chattering phenomenon at a reduced level.

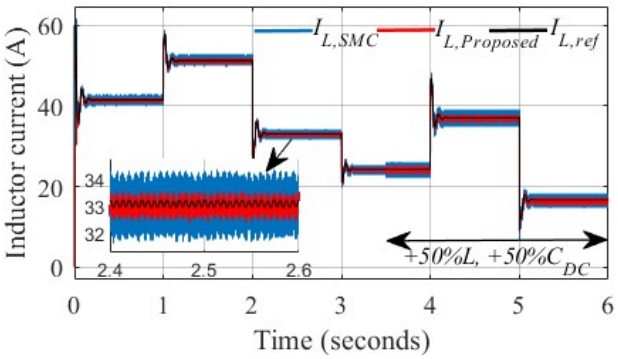

Fig. 16. Inductor current.

Fig. 17. illustrates the wind energy output power, highlighting its improved stability with lower oscillations compared to Gao's second reaching law. This reduction in ripple demonstrates the effectiveness of the proposed control strategy in minimizing power fluctuations and ensuring a smoother output, even when the DC-DC boost converter parameters are increased by +50% in both inductance L and DC-bus capacitance C_{DC}. Similarly, Fig. 18. presents the generator's electromagnetic torque, which demonstrates reduced oscillations. Moreover, it can be observed that the generator produces a high electromagnetic torque, reaching 1.8 kN.m. This high electromagnetic torque is a result of the generator's low rotational speed.

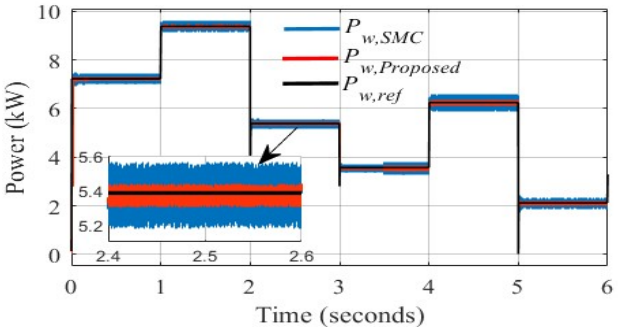

Fig. 17. Wind power.

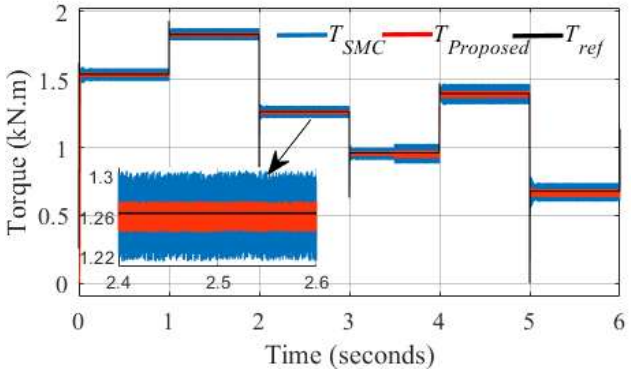

Fig. 18. Generator electromagnetic torque.

Between 2 s and 3 s, the proposed method demonstrates better dynamic performance compared to the conventional SMC approach as shown in Table.I. Specifically:

- The variation in inductor current $\Delta I_L/I_L$ is reduced to 1.8% with the Proposed method, while it reaches 6% under SMC.
- The electromagnetic torque variation $\Delta T_{em}/T_{em}$ is also much lower with the Proposed method 1.58% compared to 6.3% for SMC.
- Similarly, the output power fluctuation $\Delta P_w/P_w$ is minimized to 1.22% under the Proposed control, whereas it is 6.5% with SMC.

Table I. - Performance comparison under wind and load variation

	From 2 s to 3 s		
	$\Delta I_L/I_L$ (%)	$\Delta T_{em}/T_{em}$ (%)	$\Delta P_w/P_w$ (%)
Proposed	1.8	1.58	1.22
SMC	6	6.3	6.5

Similarly, between 2 s and 3 s, under a +50% parametric variation in both the inductance and the capacitance of the boost converter, as shown in Table II, the Proposed control method continues to outperform the convetional SMC in terms of robustness and dynamic performance:

- The relative variation in inductor current $\Delta I_L/I_L$ is limited to 2.7% with the proposed method, compared to 8.1% with SMC.
- The torque ripple $\Delta T_{em}/T_{em}$ is also significantly lower at 2.15%, while SMC exhibits a much higher variation of 7.41%.
- Similarly, the output power fluctuation $\Delta P_w/P_w$ remains controlled at 1.86% under the Proposed control, whereas it reaches 7.6% with SMC

Table II. - Performance comparison under +50% parameter Variation in Boost Converter

	From 4 s to 5 s		
	$\Delta I_L/I_L$ (%)	$\Delta T_{em}/T_{em}$ (%)	$\Delta P_w/P_w$ (%)
Proposed	2.7	2.15	1.86
SMC	8.1	7.41	7.6

Fig. 19 highlights the stability of the DC-link voltage regulation in the presence of wind speed variations, load disturbances, and parametric variations. Throughout these dynamic conditions, the voltage remains controlled around its nominal reference value of 500 V.

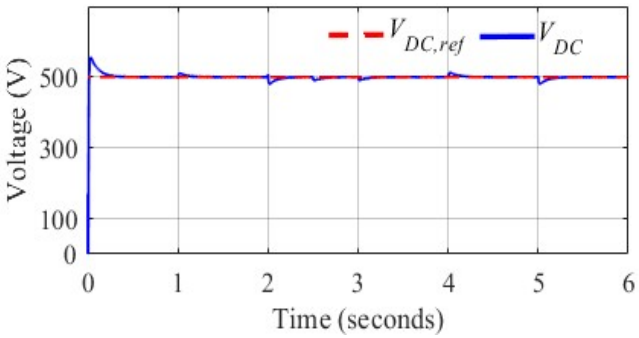

Fig. 19. DC-bus voltage.

Fig. 20 presents the battery voltage, which is regulated around its nominal value. Fig. 21. depicts the battery current, which closely tracks its reference signal. Finally, Fig. 22 depicts the evolution of the battery state of charge SOC, reflecting the reliability of the implemented energy management strategy.

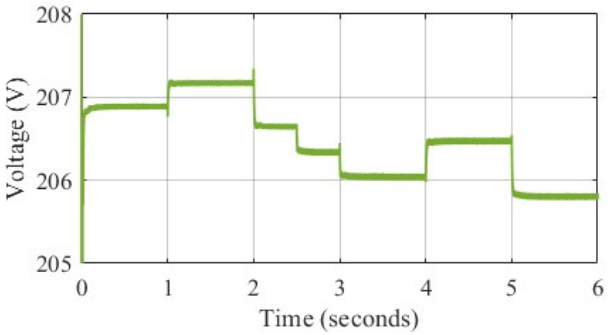

Fig. 20. Battery voltage.

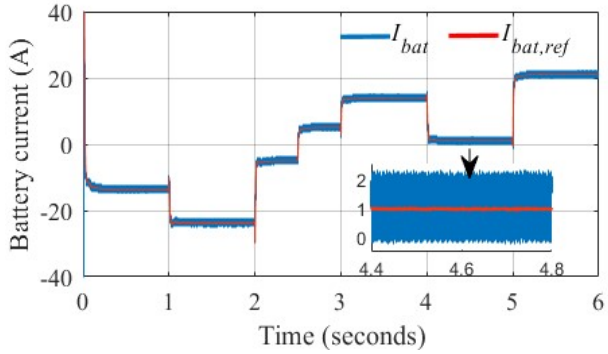

Fig. 21. Battery current.

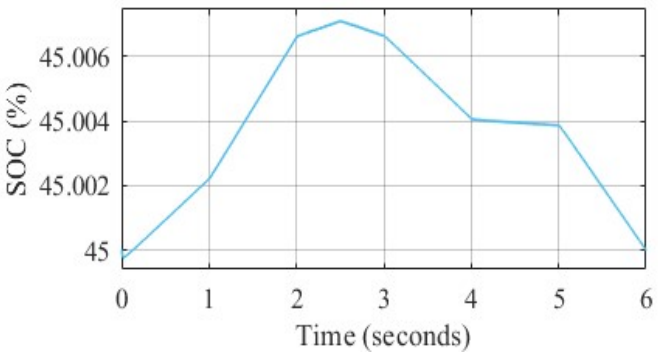

Fig. 22. Battery state of charge SOC.

Fig. 23. provides a detailed representation of the dynamics of power flow between the various components of the standalone wind turbine system, highlighting an efficient power interaction between the wind turbine, the battery storage, and the load ensuring effective energy management.

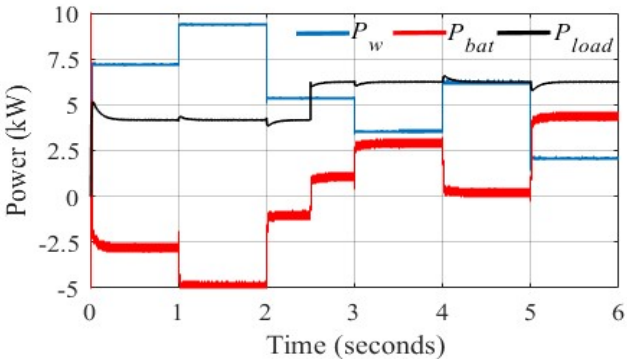

Fig. 23. Power curve.

5 . Conclusion

This paper investigates and simulates a small-scale standalone wind energy conversion system integrated with battery storage. A non-conventional direct-drive generator, characterized by low rotational speed and high electromagnetic torque, is employed to eliminate the need for a gearbox. This design choice helps overcome typical gearbox-related issues such as increased system size, cost, energy losses, and maintenance requirements.

To regulate the DC-DC boost converter, a new reaching law is introduced. The study demonstrates that the proposed control strategies significatly enhance the performance of standalone wind turbine systems. Notably, , the proposed technique reduces the chattering phenomenon in the operation of the DC-DC converter. This improvement is reflected in the reduced oscillations of both the inductor current, electromanetic torque and the output power, resulting in smoother and more stable system dynamics. These findings confirm the effectiveness and reliability of the proposed approach in the context of standalone renewable energy systems.

Moreover, the proposed control demonstrates robust performance against parameter variations in the DC-DC converter and load fluctuations, outperforming Gao's second law sliding mode control (SMC) approach. These findings confirm the effectiveness and reliability of the proposed approach in the context of standalone renewable energy systems.

References

[1] LQ. Sang, QA. Li, C. Cai, T. Maeda, Y. Kamada, et al, ‘’Wind tunnel and numerical study of a floating offshore wind turbine based on the cyclic pitch control’’, Renew Energy (2021). Vol. 172, pp.453‑464.

[2] https://www.energyinst.org/home.

[3] A. Mostafa, M. E.A. El-Hay, M.M. ELkholy, ‘’Recent Trends in Wind Energy Conversion System with Grid Integration Based on Soft Computing Methods: Comprehensive Review, Comparisons and Insights’’, Arch Computat Methods Eng (2023). Vol 30, 1439–1478.

[4] HA. Behabtu, T. Coosemans, M. Berecibar, KA. Fante, AA. Kebede, JV. Mierlo, M. Messagie, ‘’Performance Evaluation of Grid-Connected Wind Turbine Generators’’, Energies (2021). Vol. 14, pp.20:6807.
[5] A. Redouane, R. Saou, C. Guerroudj, A. Oukaour, “Enhancing wind power conversion efficiency with Vernier DSPM generator and sliding mode control ”, J. Ren. Energies (2024). Vol. 1, pp. 59.
[6] A. Redouane, R. Saou, Y. Belkhier, A. Oukaour, ‘’Integration Of a Novel Vernier-DSPM Generator in a Grid Connected Hybrid Renewable Energy System with Battery Storage’’, Results in Engineering (2025). Vol. 25, p. 103814.
[7] M. Leso, J. Zilkova and P. Girovsky, ‘’Development of a Simple Fuzzy Logic Controller for DC-DC Converter’’, IEEE 18th International Power Electronics and Motion Control Conference (2018), pp. 86-93.
[8] H. Mollaee, SM. Ghamari, SA. Saadat, AH. Seyyed, et al, ‘’A novel adaptive cascade controller design on a buck–boost DC–DC converter with a fractional-order PID voltage controller and a self-tuning regulator adaptive current controller’’, IET Power Electronics (2021). Vol. 14, p. 1920-1935.
[9] Y. Yin, et al, ‘’Backstepping Control of a DC-DC Boost Converters Under Unknown Disturbances’’, IECON-44th Annual Conference of the IEEE Industrial Electronics Society (2018), pp. 1055-1060.
[10] IA. Ayad, E. Elwarraki, A. Syed Umaid, et al, ‘’Optimized nonlinear integral backstepping controller for DC–DC three-level boost converters’’, IEEE Access (2023). Vol. 11, p. 49794-49805.
[11] YM. Alsmadi, V. Utkin, MA. Haj-Ahmed, et al, ‘’Sliding mode control of power converters: DC/DC converters’’, International Journal of Control (2018). Vol. 91, pp. 2472-2493.
[12] S. Das, MS. Qureshi, P. Swarnkar, ‘’Design of integral sliding mode control for DC-DC converters’’, Materials Today: Proceedings (2018). Vol. 5, pp. 4290-4298.
[13] R. Saou, M. E. Zaïm, K. Alitouche, ‘’Optimal Designs and Comparison of the Doubly Salient Permanent Magnet Machine and Flux-reversal Machine in Low-speed Applications’’, Electric Power Components and Systems (2008). Vol36, pp: 914-931.
[14] C. Guerroudj, R. Saou, A. Boulayoune, M. E. Zaïm, L. Moreau, ‘’Performance analysis of Vernier slotted doubly salient permanent magnet generator for wind power’’, International Journal of Hydrogen Energy (2017). Vol 13, pp: 8744-8755.
[15] N. Khosravi, M. Dowlatabadi, M. B. Abdelghany, M. Tostado-Véliz, F. Jurado, ‘’Enhancing battery management for HEVs and EVs: A hybrid approach for parameter identification and voltage estimation in lithium-ion battery models’’, Applied Energy (2024). Vol. 356, p.122364.
[16] X. Lai, M. Yuan, X. Tang, Y. Zheng, J. Zhu, Y. Sun, F. Gao, ‘’State-of-power estimation for lithium-ion batteries based on a
frequency-dependent integer-order model’’, Journal of Power Sources (2024). Vol. 594, p.234000.
[17] A. D. Falehi, H. Torkaman, ‘’Promoted supercapacitor control scheme based on robust fractional-order super-twisting sliding mode control for dynamic voltage restorer to enhance FRT and PQ capabilities of DFIG-based wind turbine’’, Journal of Energy Storage (2021). Vol. 42 p. 102983.
[18] A. Bartoszewicz A. ‘’new reaching law for sliding mode control of continuous time systems with constraints’’. Transactions of the Institute of Measurement and Control (2014). Vol.37, pp:515-521.